

Mass constraints, production cross sections, and decay rates in the Two Higgs Doublet Model of type II

Carlos A. Marín and B. Hoeneisen

Universidad San Francisco de Quito
5 February 2004

Abstract

We calculate masses, production cross sections, and decay rates in the Two Higgs Doublet Model of type II. We also discuss running coupling constants and Grand Unification. The most interesting production channels are $gg \rightarrow h^0, H^0, A^0$ on mass shell, and $q\bar{q}, gg \rightarrow h^0Z$ and $q\bar{q}' \rightarrow h^0W^\pm$ in the continuum (tho there may be peaks at m_{A^0}). The most interesting decays are $h^0, H^0, A^0 \rightarrow b\bar{b}$ -jets and $\tau^+\tau^-$, and, if above threshold, $H^0 \rightarrow ZZ, W^+W^-$ and h^0h^0 . The following final states should be compared with the Standard Model cross section: $b\bar{b}Z, b\bar{b}W^\pm, \tau^+\tau^-Z, \tau^+\tau^-W^\pm, b\bar{b}, \tau^+\tau^-, ZZ, W^+W^-, 3$ and 4 b -jets, $2\tau^+ + 2\tau^-$, $b\bar{b}\tau^+\tau^-$, ZW^+W^- , $3Z$, ZZW^\pm and $3W^\pm$. Mass peaks should be searched in the following channels: $Zb\bar{b}, ZZ, ZZZ, b\bar{b}, 4b$ -jets and, just in case, $Z\gamma$.

Contents

1	Introduction	2
2	Masses	3
3	Feynman rules	3
4	Decay rates of h^0	8
5	Branching fractions of h^0	12
6	Decay rates of H^\pm	12

7 Decays of H^0.	13
8 Decay rates of A^0	15
9 Decay $Z \rightarrow h^0\gamma$	23
10 Vertex with four particles	24
11 Production of h^0, H^0 and A^0	26
12 Production of h^0Z^0X	26
13 Production of H^+	30
14 Production of h^0W^+X	30
15 Numerical examples	32
16 Running coupling constants and Grand Unification	36
17 Conclusions	37

1 Introduction

Among the extensions of the Standard Model that respect its principles and symmetries, and are compatible with present data within a region of parameter space, and are of interest at the large particle colliders, is the addition of a second doublet of higgs fields. In this article we consider the Two Higgs Doublet Model of type II[1]. The higgs sector of the Minimal Supersymmetric Standard Model (MSSM) is of this type (tho the model of type II does not require Supersymmetry). The physical spectrum of the model contains five higgs bosons: one pseudoscalar A^0 (CP-odd scalar), two neutral scalars H^0 and h^0 (CP-even scalars), and two charged scalars H^+ and H^- . The masses of the charged Higgs bosons m_H , and the ratio of the vacuum expectation values of the two neutral components of the Higgs doublets, $\tan\beta > 0$, are free parameters of the theory.

In [2] we obtained limits in the $(m_H, \tan\beta)$ plane using measured decay rates, mixing and CP violation of mesons. In this article we present graphically the corresponding limits on m_{H^0} , m_{h^0} and m_{A^0} . Then we calculate production cross sections, decay rates and branching fractions of the higgs particles. Next, we obtain the running coupling constants and discuss

Grand Unification. Finally, in the Conclusions, we list interesting discovery channels.

2 Masses

The masses of the neutral higgs particles as a function of the masses of the charged higgs m_H , $\tan \beta$ and the masses of Z and W , calculated at tree level, are:

$$m_{A^0}^2 = m_H^2 - m_W^2, \quad (1)$$

$$2m_{H^0}^2 = m_H^2 - m_W^2 + m_Z^2 + \left[(m_H^2 - m_W^2 + m_Z^2)^2 - 4m_Z^2(m_H^2 - m_W^2) \left(\frac{\tan^2 \beta - 1}{\tan^2 \beta + 1} \right)^2 \right]^{\frac{1}{2}} \quad (2)$$

$$2m_{h^0}^2 = m_H^2 - m_W^2 + m_Z^2 - \left[(m_H^2 - m_W^2 + m_Z^2)^2 - 4m_Z^2(m_H^2 - m_W^2) \left(\frac{\tan^2 \beta - 1}{\tan^2 \beta + 1} \right)^2 \right]^{\frac{1}{2}} \quad (3)$$

We have re derived these equations in agreement with the literature.[1]

In reference [2] we obtained the limits in the $(\tan \beta, m_H)$ plane shown in Figure 1. From that figure and Equations 1, 2 and 3 we obtain the limits on the masses of the neutral higgs particles shown in Figure 2.

Radiative corrections can be very large. In the MSSM the largest contributions arise from the incomplete cancellation between top and stop loops. The corresponding plot similar to Figure 2 with radiative corrections can be found in [6].

3 Feynman rules

The Lagrangian for the VHH interaction is:[1]

$$\begin{aligned} \mathcal{L}_{VHH} = & \frac{-ig}{2} W_\mu^+ \cdot H^- \overleftrightarrow{\partial}^\mu [H^0 \sin(\alpha - \beta) + h^0 \cos(\alpha - \beta) + iA^0] + \text{h.c.} \\ & - \frac{ig}{2 \cos \theta_W} Z_\mu \{ iA^0 \overleftrightarrow{\partial}^\mu [H^0 \sin(\alpha - \beta) + h^0 \cos(\alpha - \beta)] \\ & - (2 \sin^2 \theta_W - 1) \cdot H^- \overleftrightarrow{\partial}^\mu H^+ \} \end{aligned} \quad (4)$$

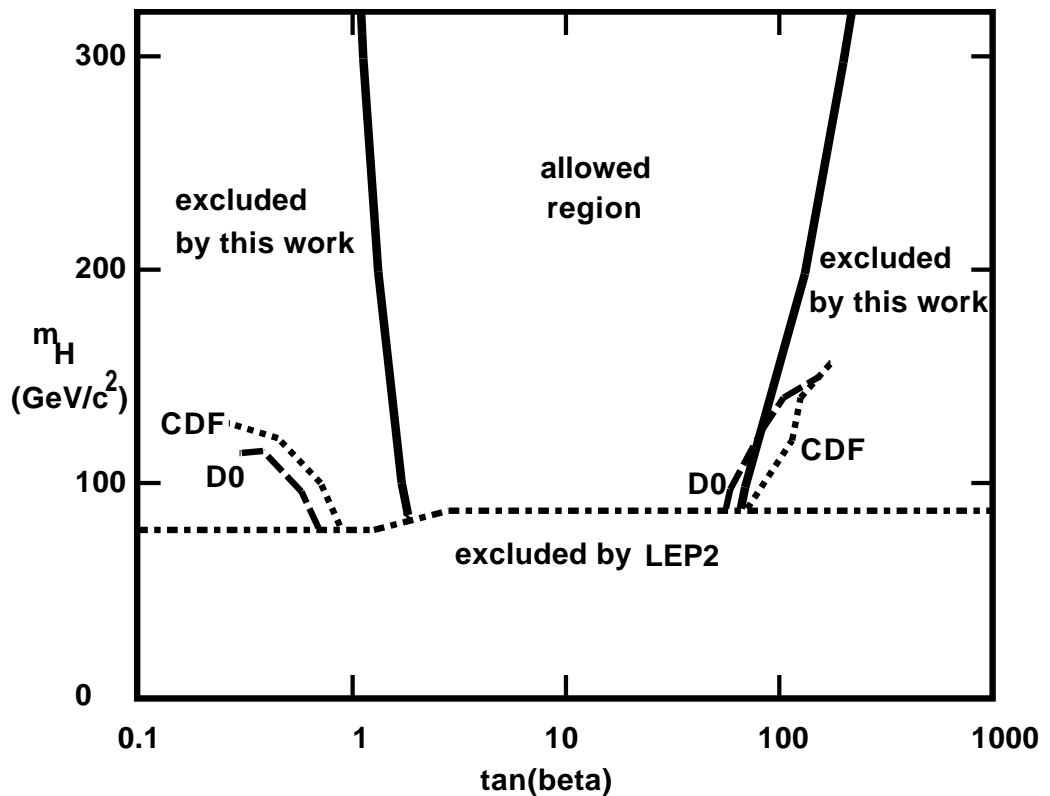


Figure 1: Lower and upper limits on $\tan \beta$ as a function of the mass of the charged higgs m_H from meson decay, mixing and CP violation (continuous curve) compared to limits obtained by CDF[3], D0[4] and LEP2[5], all at 95% confidence. Taken from [2].

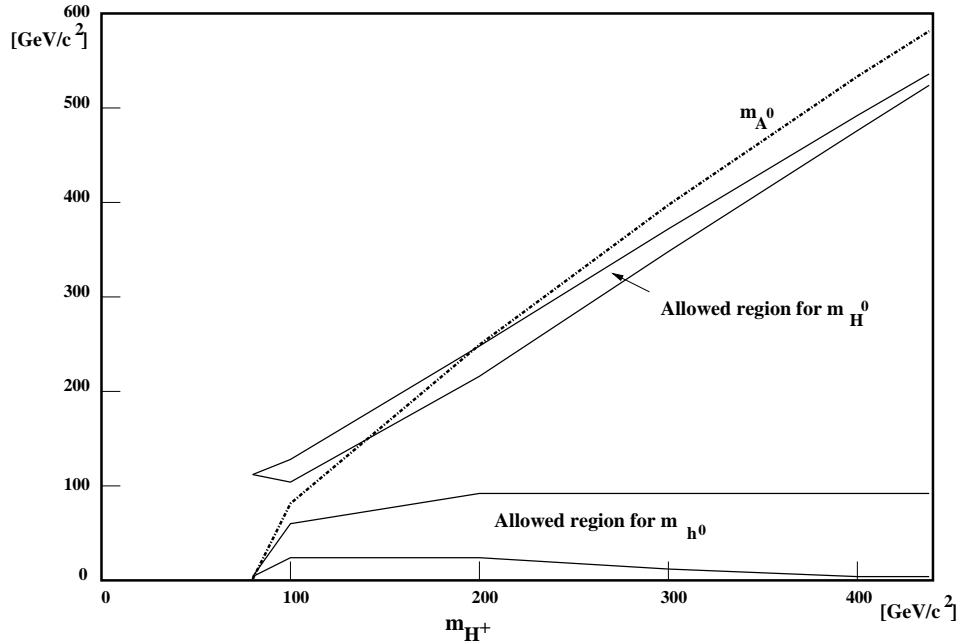


Figure 2: Allowed regions of the masses of the neutral higgs h^0 , H^0 and A^0 as a function of the mass m_H of the charged higgs H^\pm . From Figure 1 and the tree level Equations 1, 2 and 3. Radiative corrections raise the allowed region of h^0 .[6]

where

$$A \overleftrightarrow{\partial}^\mu B = A(\partial^\mu B) - (\partial^\mu A)B. \quad (5)$$

The Lagrangian for the VVH interaction is:

$$\begin{aligned} \mathcal{L}_{VVH} = & \left(g m_W W_\mu^+ W^{-\mu} + \frac{g m_Z}{2 \cos \theta_W} Z_\mu Z^\mu \right) \\ & \times [H^0 \cos(\beta - \alpha) + h^0 \sin(\beta - \alpha)]. \end{aligned} \quad (6)$$

There are no vertices ZH^0H^0 , Zh^0h^0 , ZA^0A^0 , ZW^+H^- or ZH^0h^0 . The interactions of neutral higgs bosons with up and down quarks are given by:

$$\begin{aligned} \mathcal{L}_{AHff'} = & \frac{-g m_f}{2 m_W \sin \beta} [\bar{u}_f v_{\bar{f}} (H^0 \sin \alpha + h^0 \cos \alpha) - i \cos \beta \cdot \bar{u}_f \gamma^5 v_{\bar{f}} A^0] \\ & - \frac{g m_{f'}}{2 m_W \cos \beta} \\ & \times [\bar{u}_{f'} v_{\bar{f}'} (H^0 \cos \alpha - h^0 \sin \alpha) - i \sin \beta \cdot \bar{u}_{f'} \gamma^5 v_{\bar{f}'} A^0] \end{aligned} \quad (7)$$

where $f = u, c, t, \nu_e, \nu_\mu, \nu_\tau$ and $f' = d, s, b, e^-, \mu^-, \tau^-$. The Lagrangian corresponding to the $H^\pm f \bar{f}'$ vertex is:

$$\begin{aligned} \mathcal{L}_{Hff'} = & \frac{g}{2\sqrt{2} m_W} \{ H^+ V_{ff'} \bar{u}_f (A + B \gamma^5) v_{\bar{f}'} \\ & + H^- V_{ff'}^* \bar{u}_{f'} (A - B \gamma^5) v_{\bar{f}} \} \end{aligned} \quad (8)$$

where $A \equiv (m_{f'} \tan \beta + m_f \cot \beta)$ and $B \equiv (m_{f'} \tan \beta - m_f \cot \beta)$. $V_{ff'}$ is an element of the CKM matrix. The Lagrangian corresponding to three higgs bosons is:

$$\begin{aligned} \mathcal{L}_{3h} = & -g H^0 \{ H^+ H^- \left[m_W \cos(\beta - \alpha) - \frac{m_Z}{2 \cos \theta_W} \cos(2\beta) \cos(\beta + \alpha) \right] \\ & + \frac{m_Z}{4 \cos \theta_W} H^0 H^0 \cos(2\alpha) \cos(\beta + \alpha) \\ & + \frac{m_Z}{4 \cos \theta_W} h^0 h^0 [2 \sin(2\alpha) \sin(\beta + \alpha) - \cos(\beta + \alpha) \cos(2\alpha)] \\ & - \frac{m_Z}{4 \cos \theta_W} A^0 A^0 \cos(2\beta) \cos(\beta + \alpha) \} \\ & - g h^0 \{ H^+ H^- \left[m_W \sin(\beta - \alpha) + \frac{m_Z}{2 \cos \theta_W} \cos(2\beta) \sin(\beta + \alpha) \right] \\ & + \frac{m_Z}{4 \cos \theta_W} h^0 h^0 \cos(2\alpha) \sin(\beta + \alpha) \\ & - \frac{m_Z}{4 \cos \theta_W} H^0 H^0 [2 \sin(2\alpha) \cos(\beta + \alpha) + \sin(\beta + \alpha) \cos(2\alpha)] \\ & + \frac{m_Z}{4 \cos \theta_W} A^0 A^0 \cos(2\beta) \sin(\beta + \alpha) \}. \end{aligned} \quad (9)$$

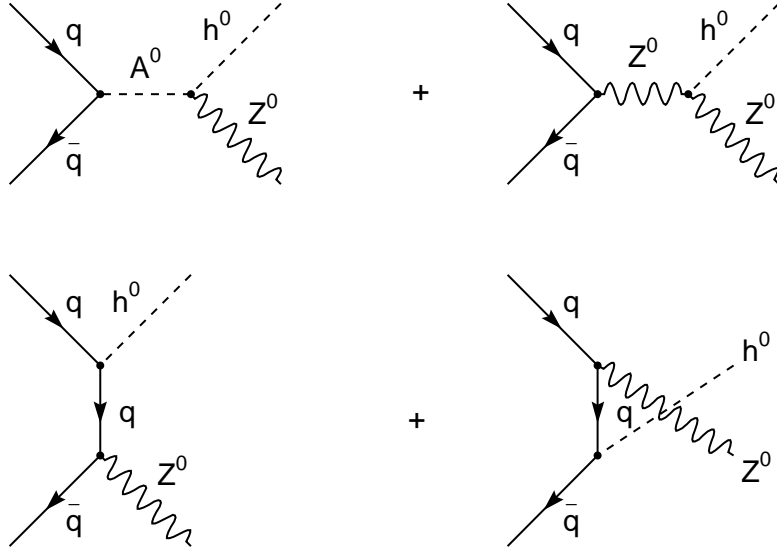


Figure 3: Feynman diagrams corresponding to the production of h^0 in the channel $q\bar{q} \rightarrow h^0 Z^0$.

Vertexes with four partons including two Higgs bosons are

$$\begin{aligned}
 \mathcal{L}_4 = & e^2 A_\mu A^\mu H^+ H^- + \frac{eg \cos(2\theta_W)}{\cos \theta_W} A_\mu Z^\mu H^+ H^- \\
 & - \frac{eg}{2} \sin(\beta - \alpha) A_\mu W^{\pm\mu} H^0 H^\mp + \frac{eg}{2} \cos(\beta - \alpha) A_\mu W^{\pm\mu} h^0 H^\mp \\
 & \pm \frac{ige}{2} A_\mu W^{\pm\mu} A^0 H^\mp,
 \end{aligned} \tag{10}$$

The $H^+ H^- \gamma$ vertex is

$$\mathcal{L}_{H^+ H^- \gamma} = -ig \sin \theta_W A_\mu H^- \overleftrightarrow{\partial}^\mu H^+ \tag{11}$$

The higgs propagators are: $i/(k^2 - m^2 + i\varepsilon)$.

Feynman diagrams corresponding to the production of $Z h^0$ are shown in Figures 3, 4 and 5. Note that the invariant mass of $Z h^0$ can have a resonance at m_{A^0} which is an interesting experimental signature. Feynman diagrams corresponding to the production of $W^\pm h^0$ or $W^\pm H^0$ are shown in Figure 6.

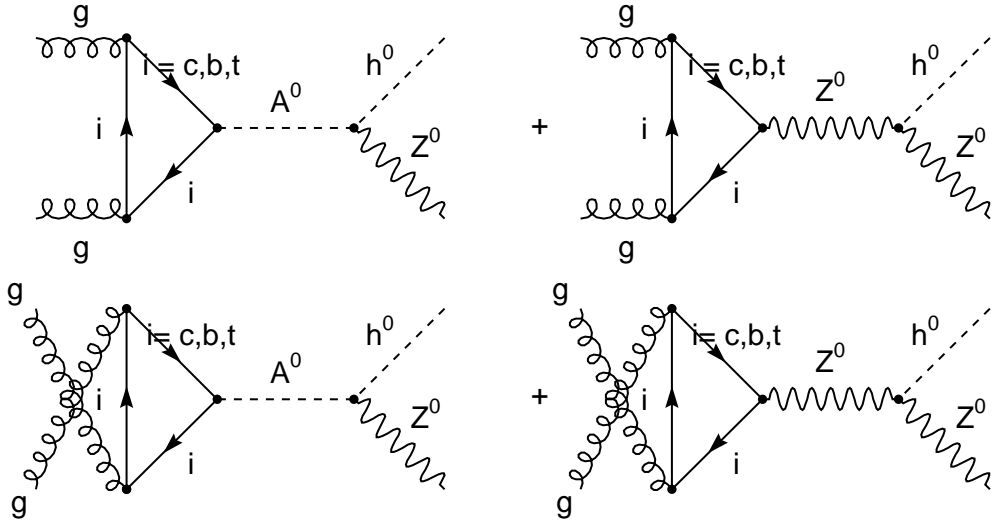


Figure 4: Feynman diagrams corresponding to the production of h^0 in the channel $gg \rightarrow h^0 Z^0$. Continued in Figure 5.

4 Decay rates of h^0

Calculating the Feynman diagrams of Figure 7 we obtain the decay rate corresponding to $h^0 \rightarrow gg$:

$$\begin{aligned} \Gamma(h^0 \rightarrow gg) = & \frac{\sqrt{2}G_F\alpha_s^2 m_{h^0}^3}{64\pi^3} \frac{\cos^2\alpha}{\sin^2\beta} |\tau_b \tan\beta \tan\alpha [(\tau_b - 1) f(\tau_b) + 2] \\ & + \tau_\tau \tan\beta \tan\alpha [(\tau_\tau - 1) f(\tau_\tau) + 2] \\ & - \tau_t [(\tau_t - 1) f(\tau_t) + 2]|^2 \end{aligned} \quad (12)$$

where

$$\tau_i = \frac{4m_i^2}{m_{h^0}^2}, \quad (13)$$

(note that τ_i will change from Section to Section),

$$f(\tau_i) = \begin{cases} -2 \left[\arcsin \left(\tau_i^{-1/2} \right) \right]^2 & \text{if } \tau_i > 1 \\ \frac{1}{2} \left[\ln \left(\frac{1+(1-\tau_i)^{1/2}}{1-(1-\tau_i)^{1/2}} \right) - i\pi \right]^2 & \text{if } \tau_i \leq 1, \end{cases} \quad (14)$$

$$\tan\alpha = \left\{ \frac{1+F}{1-F} \right\}^{\frac{1}{2}}, \quad (15)$$

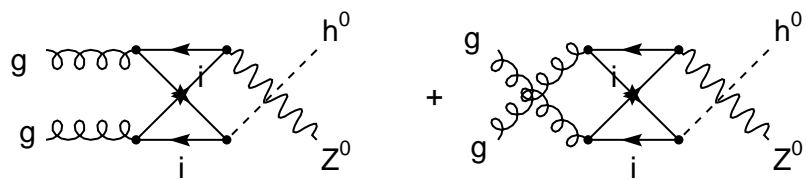
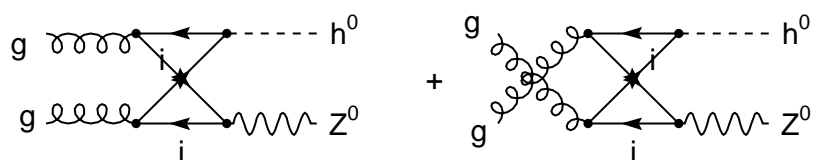
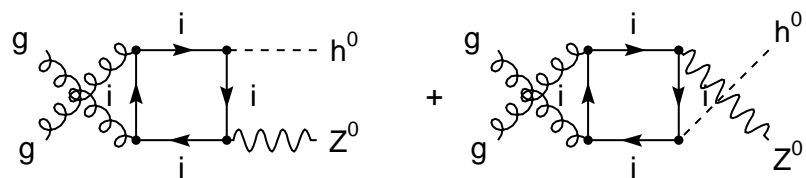
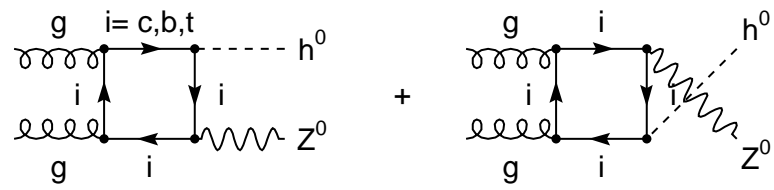


Figure 5: Continued from Figure 4.

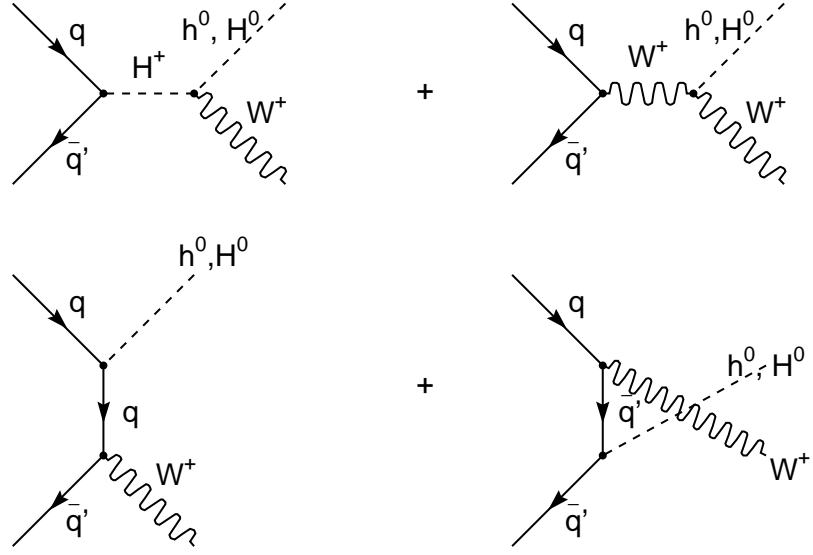


Figure 6: Feynman diagrams corresponding to the production of $h^0 W^\pm$ and $H^0 W^\pm$.

$$F = \frac{1 - \tan^2 \beta}{(1 + \tan^2 \beta) G} \left[1 - \frac{m_Z^2}{m_H^2} - \frac{m_W^2}{m_H^2} \right], \quad (16)$$

$$G = \left[\left(1 + \frac{m_Z^2}{m_H^2} - \frac{m_W^2}{m_H^2} \right)^2 - 4 \frac{m_Z^2}{m_H^2} \left(1 - \frac{m_W^2}{m_H^2} \right) \left(\frac{\tan^2 \beta - 1}{\tan^2 \beta + 1} \right)^2 \right]^{\frac{1}{2}}. \quad (17)$$

Calculating the Feynman diagrams of Figure 8 we obtain:

$$\Gamma (h^0 \rightarrow c\bar{c}) = \frac{3G_F m_c^2 m_{h^0} \cos^2 \alpha}{\sqrt{2} \cdot 4\pi \sin^2 \beta} \left(1 - \frac{4m_c^2}{m_{h^0}^2} \right)^{\frac{3}{2}}, \quad (18)$$

$$\Gamma (h^0 \rightarrow b\bar{b}) = \frac{3G_F m_b^2 m_{h^0} \sin^2 \alpha}{\sqrt{2} \cdot 4\pi \cos^2 \beta} \left(1 - \frac{4m_b^2}{m_{h^0}^2} \right)^{\frac{3}{2}}, \quad (19)$$

and

$$\Gamma (h^0 \rightarrow \tau^-\tau^+) = \frac{G_F m_\tau^2 m_{h^0} \sin^2 \alpha}{\sqrt{2} \cdot 4\pi \cos^2 \beta} \left(1 - \frac{4m_\tau^2}{m_{h^0}^2} \right)^{\frac{3}{2}}. \quad (20)$$

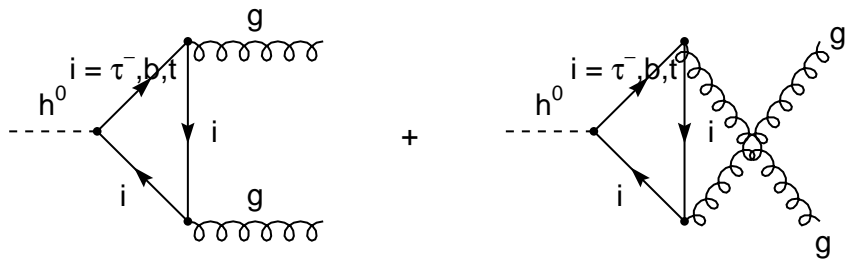


Figure 7: Feynman diagrams corresponding to the decay $h^0 \rightarrow gg$.

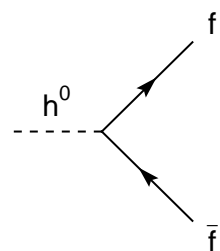


Figure 8: Feynman diagram corresponding to the decays $h^0 \rightarrow b\bar{b}, c\bar{c}, \tau\bar{\tau}$.

5 Branching fractions of h^0

From the preceding decay rates we obtain the following branching fractions for the case $m_b, m_c, m_\tau \ll m_{h^0} < 120 \text{GeV}/c^2$:

$$B(h^0 \rightarrow b\bar{b}) = \frac{3m_b^2 \sin^2 \alpha}{3m_b^2 \sin^2 \alpha + 3m_c^2 \cos^2 \alpha \cot^2 \beta + m_\tau^2 \sin^2 \alpha + J} \quad (21)$$

and

$$B(h^0 \rightarrow \tau^+ \tau^-) = \frac{m_\tau^2 \sin^2 \alpha}{3m_b^2 \sin^2 \alpha + 3m_c^2 \cos^2 \alpha \cot^2 \beta + m_\tau^2 \sin^2 \alpha + J} \quad (22)$$

where

$$\begin{aligned} J = & \frac{\alpha_s^2 m_{h^0}^2 \cos^2 \alpha}{8\pi^2 \tan^2 \beta} |\tan \beta \tan \alpha \sum_{j=b,\tau} \left[\tau_j \left(-\frac{1}{2} \left\{ \ln \left(\frac{\tau_j}{4} \right) + i\pi \right\}^2 + 2 \right) \right. \\ & \left. - \tau_t \{(\tau_t - 1) f(\tau_t) + 2\} \right|^2. \end{aligned} \quad (23)$$

For $90 < m_H < 1000 \text{GeV}/c^2$, $B(h^0 \rightarrow b\bar{b})$ varies from 0.856 to 0.944. Neglecting $B(h^0 \rightarrow gg)$ and the contribution of $c\bar{c}$ we obtain

$$B(h^0 \rightarrow b\bar{b}) = \frac{3m_b^2}{3m_b^2 + m_\tau^2} = 0.944 \quad (24)$$

and

$$B(h^0 \rightarrow \tau^+ \tau^-) = \frac{m_\tau^2}{3m_b^2 + m_\tau^2} = 0.056. \quad (25)$$

6 Decay rates of H^\pm

The tree level Feynman diagram of Figure 9 gives the following decay rate:

$$\begin{aligned} \Gamma(H^\pm \rightarrow W^\pm h^0) = & \frac{\sqrt{2}G_F \cos^2 \alpha}{16\pi m_H^3 (1 + \tan^2 \beta)} [1 + \tan \beta \tan \alpha]^2 \\ & \times \Lambda^{3/2}(m_H^2, m_W^2, m_{h^0}^2) \end{aligned} \quad (26)$$

where

$$\Lambda(a, b, c) = a^2 + b^2 + c^2 - 2ab - 2bc - 2ca. \quad (27)$$

Similarly from the Feynman diagrams of Figures 10 and 11 we obtain

$$\begin{aligned} \Gamma(H^\pm \rightarrow W^\pm H^0) = & \frac{\sqrt{2}G_F (\tan \beta - \tan \alpha)^2}{16\pi m_H^3 (1 + \tan^2 \beta) (1 + \tan^2 \alpha)} \\ & \times \Lambda^{3/2}(m_H^2, m_W^2, m_{H^0}^2), \end{aligned} \quad (28)$$

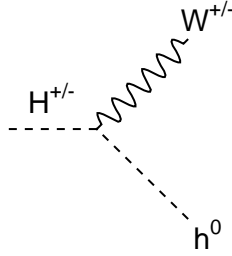


Figure 9: Feynman diagram corresponding to the decay $H^\pm \rightarrow W^\pm h^0$.

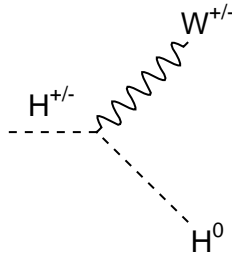


Figure 10: Feynman diagram corresponding to the decay $H^\pm \rightarrow W^\pm H^0$.

$$\Gamma(H^\pm \rightarrow W^\pm A^0) = \frac{\sqrt{2}G_F}{16\pi m_H^3} \Lambda^{3/2} (m_{A^0}^2, m_W^2, m_H^2). \quad (29)$$

7 Decays of H^0 .

The tree level Feynman diagrams of Figure 12 give the following decay rates:

$$\Gamma(H^0 \rightarrow f\bar{f}) = \frac{\sqrt{2}G_F m_f^2 m_{H^0}}{8\pi} \left(1 - \frac{4m_f^2}{m_{H^0}^2}\right)^{3/2} N_f B_f^2 \quad (30)$$

where $N_f = 3$ for quarks, $N_f = 1$ for leptons, $B_f^2 = \sin^2 \alpha (1 + \cot^2 \beta)$ for $f = u, c, t$, and $B_f^2 = \cos^2 \alpha (1 + \tan^2 \beta)$ for $f = d, s, b, e^-, \mu^-, \tau^-$.

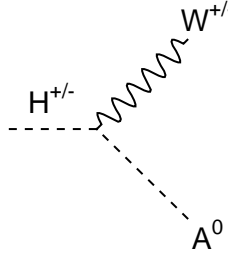


Figure 11: Feynman diagram corresponding to the decay $H^\pm \rightarrow W^\pm A^0$.

From the Feynman diagrams of Figure 13 we obtain

$$\begin{aligned} \Gamma(H^0 \rightarrow gg) = & \frac{\sqrt{2}G_F\alpha_s^2 m_{H^0}^3}{64\pi^3} \sin^2 \alpha (1 + \cot^2 \beta) \\ & \left| \frac{\tan \beta}{\tan \alpha} \sum_{i=b,\tau} \tau_i [(\tau_i - 1)f(\tau_i) + 2] \right. \\ & \left. + \tau_t [(\tau_t - 1)f(\tau_t) + 2] \right|^2 \end{aligned} \quad (31)$$

where

$$\tau_i = \frac{4m_i^2}{m_{H^0}^2}. \quad (32)$$

From the Feynman diagram of Figure 14 we obtain

$$\begin{aligned} \Gamma(H^0 \rightarrow h^0 h^0) = & \frac{\sqrt{2}G_F m_Z^4}{32\pi m_{H^0}} \left(1 - \frac{4m_{h^0}^2}{m_{H^0}^2}\right)^{1/2} \frac{(1 - \tan^2 \alpha)^2}{(1 + \tan^2 \alpha)^3 (1 + \tan^2 \beta)} \\ & \left[\frac{4 \tan \alpha}{1 - \tan^2 \alpha} (\tan \alpha + \tan \beta) - (1 - \tan \alpha \tan \beta) \right]^2. \end{aligned} \quad (33)$$

From the Feynman diagrams of Figures 15 and 16 we obtain

$$\begin{aligned} \Gamma(H^0 \rightarrow A^0 A^0) = & \frac{\sqrt{2}G_F m_Z^4}{32\pi m_{H^0}} \left(1 - \frac{4m_{A^0}^2}{m_{H^0}^2}\right)^{1/2} \\ & \frac{(\tan^2 \beta - 1)^2}{(1 + \tan^2 \alpha)^3 (1 + \tan^2 \beta)^3} [1 - \tan \alpha \tan \beta]^2, \end{aligned} \quad (34)$$

$$\begin{aligned} \Gamma(H^0 \rightarrow ZZ) = & \frac{\sqrt{2}G_F (1 + \tan \beta \tan \alpha)^2 m_{H^0}^3}{32\pi (1 + \tan^2 \beta) (1 + \tan^2 \alpha)} \\ & \times (12x^2 - 4x + 1) (1 - 4x)^{1/2} \end{aligned} \quad (35)$$

where

$$x = \frac{m_Z^2}{m_{H^0}^2}. \quad (36)$$

Similarly, from the diagram of Figure 17 we obtain

$$\begin{aligned} \Gamma(H^0 \rightarrow W^+ W^-) &= \frac{\sqrt{2}G_F (1 + \tan \beta \tan \alpha)^2 m_{H^0}^3}{16\pi (1 + \tan^2 \beta) (1 + \tan^2 \alpha)} \\ &\times (12y^2 - 4y + 1) (1 - 4y)^{1/2} \end{aligned} \quad (37)$$

where

$$y = \frac{m_W^2}{m_{H^0}^2}. \quad (38)$$

From the Feynman diagram of Figure 18 we obtain

$$\begin{aligned} \Gamma(H^0 \rightarrow W^\pm H^\mp) &= \frac{\sqrt{2}G_F (\tan \alpha - \tan \beta)^2}{16\pi m_{H^0}^3 (1 + \tan^2 \alpha) (1 + \tan^2 \beta)} \\ &\times \Lambda^{3/2} (m_{H^0}^2, m_W^2, m_H^2). \end{aligned} \quad (39)$$

From the Feynman diagram of Figure 19 we obtain

$$\begin{aligned} \Gamma(H^0 \rightarrow H^+ H^-) &= \frac{\sqrt{2}G_F m_W^4}{4\pi m_{H^0} (1 + \tan^2 \beta) (1 + \tan^2 \alpha)} \\ &\times \left[(1 + \tan \beta \tan \alpha) - \frac{(1 - \tan \beta \tan \alpha)}{2 \cos^2 \theta_W} \frac{1 - \tan^2 \beta}{1 + \tan^2 \beta} \right]^2 \\ &\times \left(1 - \frac{4m_H^2}{m_{H^0}^2} \right)^{1/2}. \end{aligned} \quad (40)$$

The Feynman diagrams corresponding to $h^0, H^0 \rightarrow \gamma\gamma$ are shown in Figure 20.

$$\Gamma(H^0 \rightarrow h^0 Z) = 0. \quad (41)$$

8 Decay rates of A^0

From the tree level Feynman diagram of Figure 21 we obtain

$$\Gamma(A^0 \rightarrow Z h^0) = \frac{\sqrt{2}G_F \cos^2 \alpha}{16\pi m_{A^0}^3 (1 + \tan^2 \beta)} [1 + \tan \beta \tan \alpha]^2 \Lambda^{3/2} (m_{A^0}^2, m_{h^0}^2, m_Z^2). \quad (42)$$

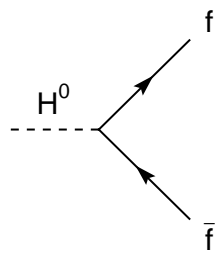


Figure 12: Feynman diagram corresponding to the decay $H^0 \rightarrow f\bar{f}$.

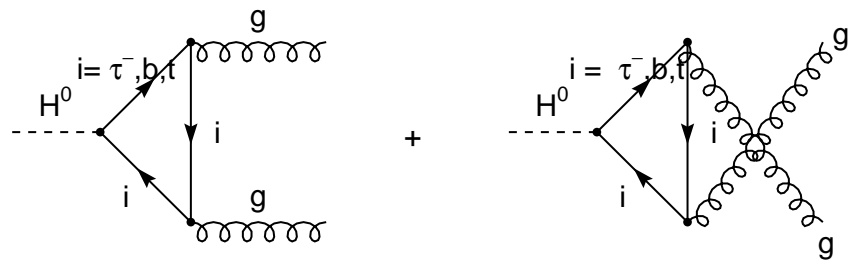


Figure 13: Feynman diagrams corresponding to the decay $H^0 \rightarrow gg$.

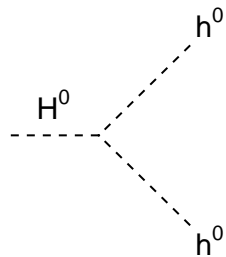


Figure 14: Feynman diagram corresponding to the decay $H^0 \rightarrow h^0 h^0$.

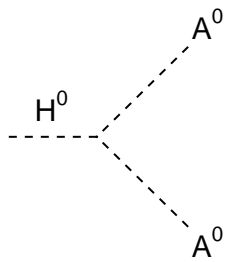


Figure 15: Feynman diagram corresponding to the decay $H^0 \rightarrow A^0 A^0$.

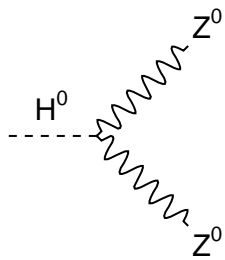


Figure 16: Feynman diagram corresponding to the decay $H^0 \rightarrow ZZ$.

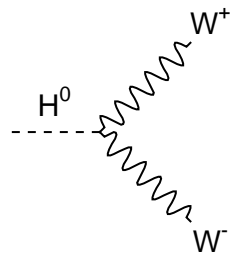


Figure 17: Feynman diagram corresponding to the decay $H^0 \rightarrow W^+ W^-$.

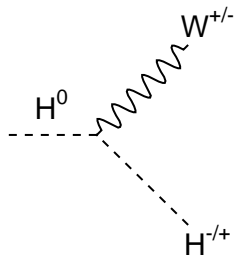


Figure 18: Feynman diagram corresponding to the decay $H^0 \rightarrow W^\pm H^\mp$.

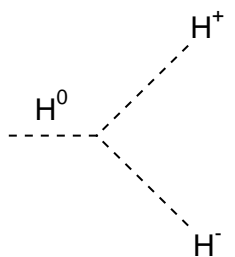


Figure 19: Feynman diagram corresponding to the decay $H^0 \rightarrow H^+ H^-$.

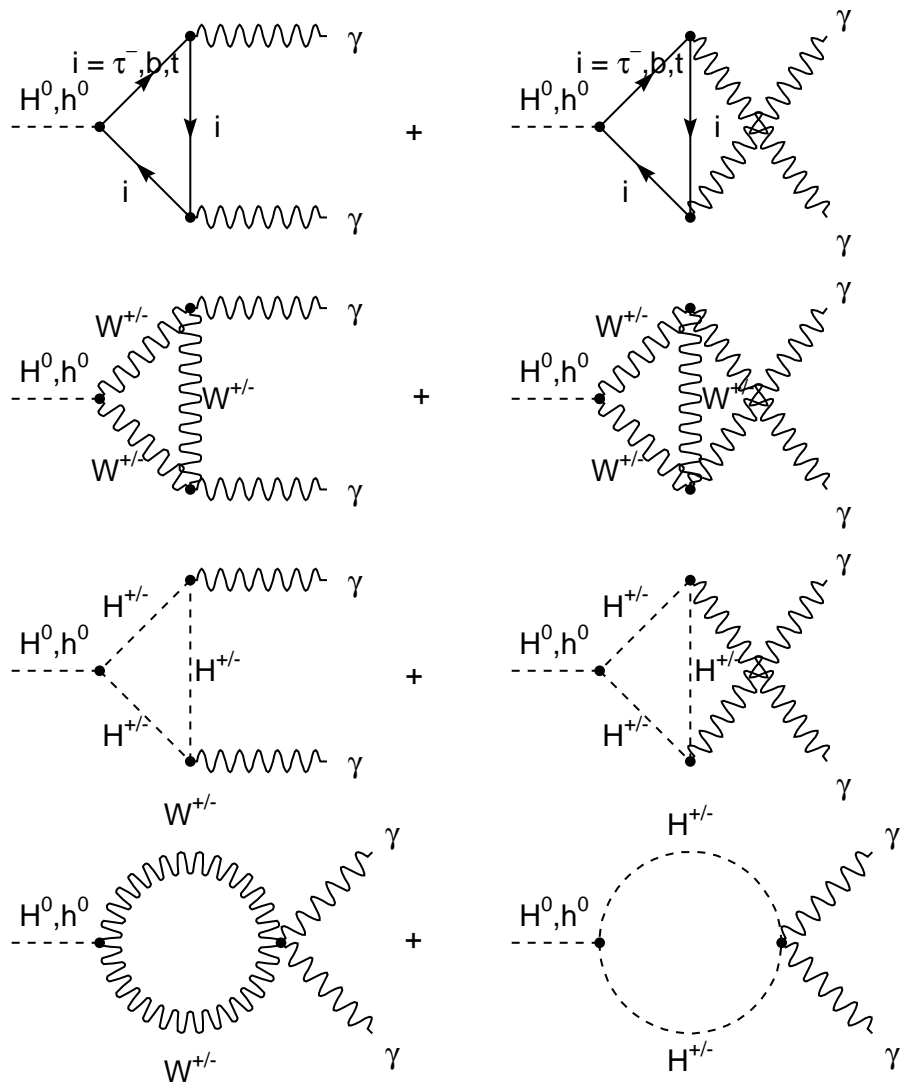


Figure 20: Feynman diagrams corresponding to $h^0, H^0 \rightarrow \gamma\gamma$.

From the tree level diagram of Figure 22 we obtain

$$\Gamma(A^0 \rightarrow f\bar{f}) = \frac{\sqrt{2}G_F}{8\pi} m_{A^0} m_f^2 A_f^2 \left(1 - \frac{4m_f^2}{m_{A^0}^2}\right)^{1/2} N_f \quad (43)$$

where $N_f = 3$ for quarks, $N_f = 1$ for leptons, $A_f = \cot\beta$ for $f = u, c, t$, and $A_f = \tan\beta$ for $f = d, s, b, e^-, \mu^-, \tau^-$.

From the Feynman diagrams shown in Figure 23 we obtain:

$$\begin{aligned} \Gamma(A^0 \rightarrow Z\gamma) = & \frac{\sqrt{2}G_F \alpha_{em}^2 m_{A^0}^3}{512\pi^3 \sin^2 \theta_W \cos^2 \theta_W} \left(1 - \frac{m_Z^2}{m_{A^0}^2}\right)^3 |\tan\beta| \\ & \left[\left(\frac{1}{2} - \frac{2}{3} \sin^2 \theta_W\right) I(\tau_b, \Lambda_b) + \left(\frac{1}{2} - 2 \sin^2 \theta_W\right) I(\tau_\tau, \Lambda_\tau) \right] \\ & + 2 \cot\beta \left(\frac{1}{2} - \frac{4}{3} \sin^2 \theta_W\right) I(\tau_t, \Lambda_t) |^2 \end{aligned} \quad (44)$$

where

$$\tau_i = \frac{4m_i^2}{m_{A^0}^2}, \quad \Lambda_i = \frac{4m_i^2}{m_Z^2}, \quad (45)$$

and

$$I(\tau_i, \Lambda_i) = \frac{\tau_i \Lambda_i}{\Lambda_i - \tau_i} \{f(\tau_i) - f(\Lambda_i)\}. \quad (46)$$

From the Feynman diagrams of Figure 24 we obtain the decay rate:

$$\Gamma(A^0 \rightarrow gg) = \frac{\sqrt{2}G_F \alpha_s^2 m_{A^0}^3}{128\pi^3} |\tan\beta \sum_{i=b,\tau} \tau_i f(\tau_i) + \cot\beta \tau_t f(\tau_t)|^2. \quad (47)$$

$$\Gamma(A^0 \rightarrow h^0 h^0) = \Gamma(A^0 \rightarrow H^0 H^0) = 0. \quad (48)$$

From the Feynman diagram 25 we obtain

$$\Gamma(A^0 \rightarrow W^\pm H^\mp) = \frac{\sqrt{2}G_F}{16\pi m_{A^0}^3} \Lambda^{3/2} (m_{A^0}^2, m_W^2, m_H^2). \quad (49)$$

From the Feynman diagram 26 we obtain

$$\begin{aligned} \Gamma(A^0 \rightarrow ZH^0) = & \frac{\sqrt{2}G_F (\tan\beta - \tan\alpha)^2}{16\pi m_{A^0}^3 (1 + \tan^2 \alpha) (1 + \tan^2 \beta)} \\ & \times \Lambda^{3/2} (m_{A^0}^2, m_{H^0}^2, m_Z^2). \end{aligned} \quad (50)$$

From the Feynman diagrams of 27 we obtain:

$$\begin{aligned} \Gamma(A^0 \rightarrow \gamma\gamma) = & \frac{\sqrt{2}G_F \alpha_{em}^2 m_{A^0}^3}{256\pi^3} \\ & \times \left| \tan\beta \left[\frac{1}{3} \tau_b f(\tau_b) + \tau_\tau f(\tau_\tau) \right] + \cot\beta \left[\frac{4}{3} \tau_t f(\tau_t) \right] \right|^2 \end{aligned} \quad (51)$$

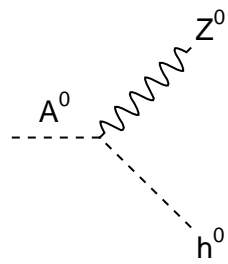


Figure 21: Feynman diagram corresponding to the decay $A^0 \rightarrow Z h^0$.

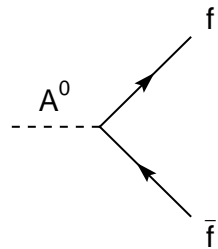


Figure 22: Feynman diagram corresponding to the decay $A^0 \rightarrow f \bar{f}$.

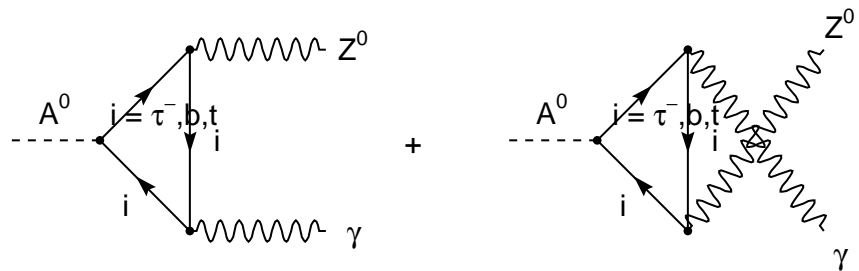


Figure 23: Feynman diagrams corresponding to the decay $A^0 \rightarrow Z \gamma$.

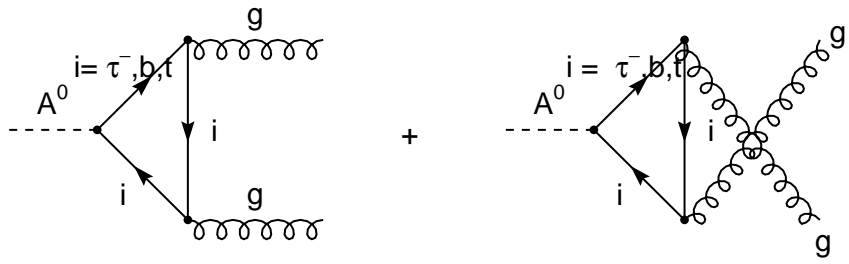


Figure 24: Feynman diagrams of $A^0 \rightarrow gg$.

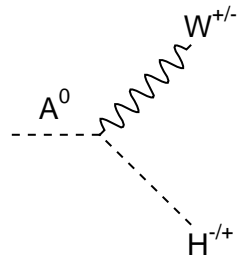


Figure 25: Feynman diagram of $A^0 \rightarrow W^\pm H^\mp$.

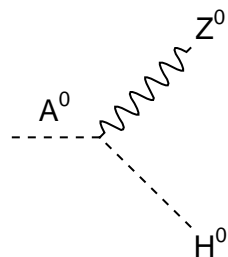


Figure 26: Feynman diagram of $A^0 \rightarrow ZH^0$.

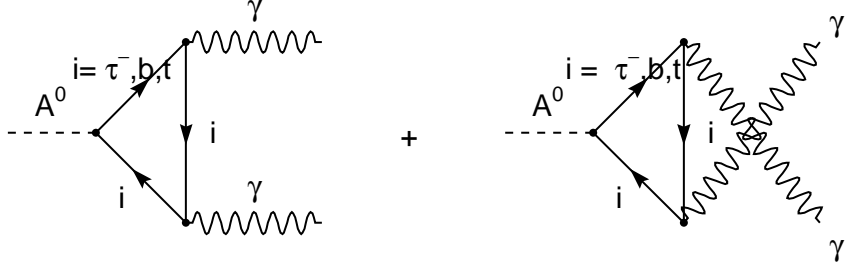


Figure 27: Feynman diagrams for $A^0 \rightarrow \gamma\gamma$.

9 Decay $Z \rightarrow h^0\gamma$

From the Feynman diagrams of Figure 28 we obtain:

$$\begin{aligned}
 \Gamma(Z \rightarrow h^0\gamma) = & \frac{\sqrt{2}G_F\alpha_{em}^2 m_Z^3}{64\pi^3 \sin^2 \theta_W \cos^2 \theta_W} \left(1 - \frac{m_{h^0}^2}{m_Z^2}\right)^3 \cos^2 \alpha \cos^2 \beta \\
 & \left| \frac{1}{\cos \beta \sin \beta} [\tan \alpha \tan \beta \left(\frac{1}{2} - \frac{2}{3} \sin^2 \theta_W\right) F(\tau_b, \Lambda_b) \right. \\
 & + \tan \alpha \tan \beta \left(\frac{1}{2} - 2 \sin^2 \theta_W\right) F(\tau_\tau, \Lambda_\tau) \\
 & - 2 \left(\frac{1}{2} - \frac{4}{3} \sin^2 \theta_W\right) F(\tau_t, \Lambda_t)] \\
 & + \left[\tan \beta - \tan \alpha + \frac{1 - \tan^2 \beta}{1 + \tan^2 \beta} \frac{\tan \beta + \tan \alpha}{2 \cos^2 \theta_W} \right] \\
 & \times \frac{m_W^2}{2m_H^2} (1 - 2 \sin^2 \theta_W) I(\tau_H, \Lambda_H) \\
 & - \frac{1}{2} (\tan \beta - \tan \alpha) \cos^2 \theta_W [4 (3 - \tan^2 \theta_W) K(\tau_W, \Lambda_W) \\
 & \left. + \left\{ \left(1 + \frac{2}{\tau_W}\right) \tan^2 \theta_W - \left(5 + \frac{2}{\tau_W}\right) \right\} I(\tau_W, \Lambda_W)] \right|^2 \quad (52)
 \end{aligned}$$

where

$$\tau_i = \frac{4m_i^2}{m_{h^0}^2}, \quad \Lambda_i = \frac{4m_i^2}{m_Z^2}, \quad \tau_H = \frac{4m_H^2}{m_{h^0}^2}, \quad \Lambda_H = \frac{4m_H^2}{m_Z^2}, \quad (53)$$

$$\begin{aligned}
F(\tau_i, \Lambda_i) &= -\frac{1}{2} \frac{\tau_i \Lambda_i}{\tau_i - \Lambda_i} - \frac{\tau_i^2 \Lambda_i}{(\tau_i - \Lambda_i)^2} \{g(\tau_i) - g(\Lambda_i)\} \\
&\quad + \frac{1}{4} \frac{\tau_i \Lambda_i}{\tau_i - \Lambda_i} \left[1 + \frac{\tau_i \Lambda_i}{\tau_i - \Lambda_i} \right] \{f(\tau_i) - f(\Lambda_i)\}, \tag{54}
\end{aligned}$$

$$g(x) = \begin{cases} (x-1)^{1/2} \arcsin(x^{-1/2}) & \text{if } x \geq 1 \\ \frac{1}{2} (1-x)^{1/2} \left[\ln \left\{ \frac{1+(1-x)^{1/2}}{1-(1-x)^{1/2}} \right\} - i\pi \right] & \text{if } x < 1, \end{cases} \tag{55}$$

$$\begin{aligned}
I(\tau_H, \Lambda_H) &= -\frac{1}{2} \frac{\tau_H \Lambda_H}{(\tau_H - \Lambda_H)} - \frac{\tau_H^2 \Lambda_H}{(\tau_H - \Lambda_H)^2} [g(\tau_H) - g(\Lambda_H)] \\
&\quad + \frac{1}{4} \frac{\tau_H^2 \Lambda_H^2}{(\tau_H - \Lambda_H)^2} [f(\tau_H) - f(\Lambda_H)], \tag{56}
\end{aligned}$$

$$\tau_W = \frac{4m_W^2}{m_{h^0}^2}, \quad \Lambda_W = \frac{4m_W^2}{m_Z^2}, \tag{57}$$

$$K(\tau_W, \Lambda_W) = -\frac{\tau_W \Lambda_W}{4(\tau_W - \Lambda_W)} [f(\tau_W) - f(\Lambda_W)]. \tag{58}$$

The decay width of Equation 52 turns out to be negligible compared to the full width of Z so we can not use it to constrain the mass of h^0 .

10 Vertex with four particles

The decay rate corresponding to the Feynman diagram 29 is:

$$\begin{aligned}
\Gamma(H^\pm \rightarrow W^\pm \gamma h^0) &= \frac{3G_F^2 \sin^2 \theta_W (1 + \tan \beta \tan \alpha)^2 m_W^5}{32 (1 + \tan^2 \beta) (1 + \tan^2 \alpha) \pi^3 (x_H^W)^{1/2}} \\
&\quad \times \left\{ \frac{1}{2} \Lambda^{\frac{1}{2}} \left(1, x_H^W, x_H^{h^0} \right) \left(1 + x_H^W + x_H^{h^0} \right) \right. \\
&\quad + \left(2x_H^W x_H^{h^0} - x_H^W - x_H^{h^0} \right) \times \ln \left| \frac{\Lambda^{\frac{1}{2}} \left(1, x_H^W, x_H^{h^0} \right) + 1 - x_H^W - x_H^{h^0}}{2 (x_H^W x_H^{h^0})^{1/2}} \right| \\
&\quad - \left| x_H^{h^0} - x_H^W \right| \times \\
&\quad \left. \ln \left| \frac{\left| x_H^{h^0} - x_H^W \right| \Lambda^{\frac{1}{2}} \left(1, x_H^W, x_H^{h^0} \right) - \left(x_H^W + x_H^{h^0} \right) + \left(x_H^W - x_H^{h^0} \right)^2}{2 (x_H^W x_H^{h^0})^{1/2}} \right| \right\} \tag{59}
\end{aligned}$$

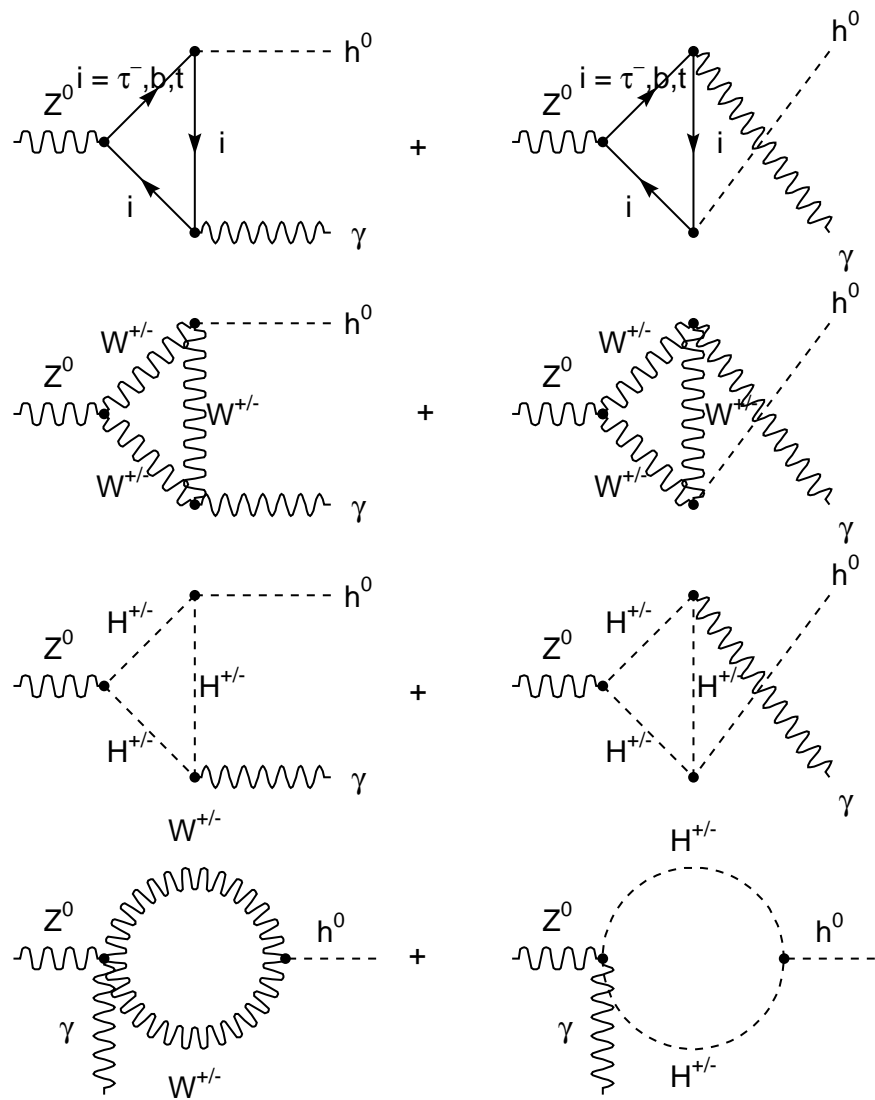


Figure 28: Feynman diagrams for $Z \rightarrow h^0\gamma$.

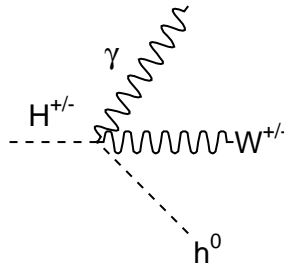


Figure 29: Diagram for $H^\pm \rightarrow W^\pm \gamma h^0$.

where

$$x_H^W = \frac{m_W^2}{m_H^2}, \quad x_H^{h^0} = \frac{m_{h^0}^2}{m_H^2}. \quad (60)$$

11 Production of h^0 , H^0 and A^0

From the Feynman diagrams in Figure 30 we obtain

$$\begin{aligned} \sigma(p\bar{p} \rightarrow AX) = & \frac{\pi^2 \Gamma(A \rightarrow 2g) \gamma_A}{8m_A^3} \int_{\gamma_A}^1 \frac{dx_a}{x_a} g(x_a, m^2) g\left(\frac{\gamma_A}{x_a}, m^2\right) \\ & + \frac{4\pi^2 \gamma_A}{3m_A^3} \left[\sum_{q=u,d,s,c,b} \Gamma(A \rightarrow q\bar{q}) \int_{\gamma_A}^1 \frac{dx_a}{x_a} f_q(x_a, m^2) f_q\left(\frac{\gamma_A}{x_a}, m^2\right) \right] \end{aligned} \quad (61)$$

where $A \equiv h^0, H^0, A^0$ and $\gamma_A \equiv m_A^2/s$. Here f_q is the unpolarized parton distribution function for quark or anti-quark q and g is the parton distribution function for gluons. m^2 is the factorization scale. $\Gamma(h^0 \rightarrow gg)$ is given by (12), $\Gamma(H^0 \rightarrow gg)$ by (31), $\Gamma(A^0 \rightarrow gg)$ by (47), $\Gamma(h^0 \rightarrow c\bar{c})$ by (18), $\Gamma(h^0 \rightarrow b\bar{b})$ by (19), $\Gamma(H^0 \rightarrow q\bar{q})$ by (30), and finally, $\Gamma(A^0 \rightarrow q\bar{q})$ is given by (43).

12 Production of $h^0 Z^0 X$

A production channel with interesting experimental signature is $p\bar{p} \rightarrow h^0 Z^0 X$. The differential cross section obtained from the Feynman diagrams in Figure

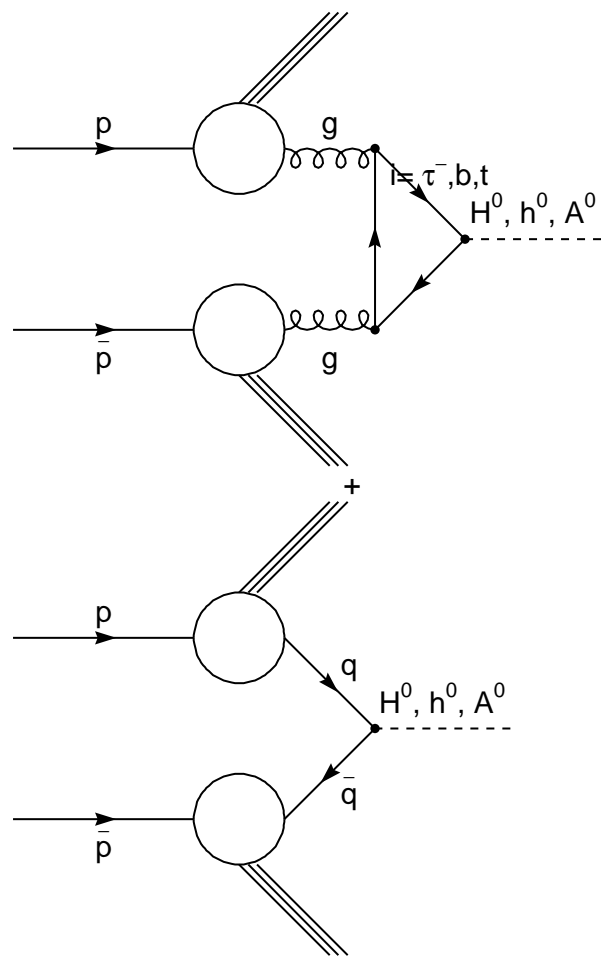


Figure 30: Feynman diagrams for $p\bar{p} \rightarrow AX$ with $A \equiv h^0, H^0, A^0$.

3 is

$$\frac{d^2\sigma}{dyd(p_T)^2} = \sum_f \int_{x_{amin}}^1 dx_a f_f(x_a, m_a^2) f_f(x_b, m_b^2) \frac{x_b \hat{s}}{m_{h^0}^2 - \hat{u}} \times \frac{d\sigma}{d\hat{t}} (f\bar{f} \rightarrow h^0 Z^0) \quad (62)$$

where f is q or g ,

$$x_{amin} = \frac{\sqrt{s}m_T e^y + m_{h^0}^2 - m_Z^2}{s - \sqrt{s}m_T e^{-y}}, \quad (63)$$

$$m_T = (m_Z^2 + p_T^2)^{\frac{1}{2}}, \quad (64)$$

$$x_b = \frac{x_a \sqrt{s}m_T e^{-y} + m_{h^0}^2 - m_Z^2}{x_a s - \sqrt{s}m_T e^y}, \quad (65)$$

$$\hat{s} = x_a x_b s, \quad (66)$$

$$p_T^2 = \frac{\Lambda(\hat{s}, m_{h^0}^2, m_Z^2) \sin^2 \theta}{4\hat{s}}, \quad (67)$$

$$\hat{u} = \frac{1}{2} (m_{h^0}^2 + m_Z^2 - \hat{s} - \cos \theta \Lambda^{1/2}(\hat{s}, m_{h^0}^2, m_Z^2)) \quad (68)$$

and

$$\hat{u}\hat{t} = m_{h^0}^2 m_Z^2 + \hat{s} p_T^2. \quad (69)$$

y is the rapidity, θ is the angle of dispersion, and p_T is the transverse momentum of Z^0 . For the light quarks u , d and s we obtain

$$\frac{d\sigma}{d\hat{t}} = \frac{1}{48\pi\hat{s}} G_F^2 m_Z^4 \frac{\sin^2(\beta - \alpha)}{(\hat{s} - m_Z^2)^2 + m_Z^2 \Gamma_Z^2} \left[(g_V^f)^2 + (g_A^f)^2 \right] \times \left[8m_Z^2 + \frac{\Lambda(\hat{s}, m_{h^0}^2, m_Z^2)}{\hat{s}} \sin^2 \theta \right] \quad (70)$$

where $g_A^f \equiv t_{3L}(f)$ and $g_V^f \equiv t_{3L}(f) - 2q_f \sin^2 \theta_W$. Coefficients in Equation (70) are given in Table 1. The Standard Model cross section is obtained by omitting the factor $\sin^2(\beta - \alpha)$ in Equation (70). The contributions to the cross section from the heavy quarks c and b are negligible. Γ_Z is the total decay width of the Z^0 .

f	$t_{3L}(f)$	q_f	g_A^f	g_V^f
e^-, μ^-, τ^-	$-\frac{1}{2}$	-1	$-\frac{1}{2}$	$-\frac{1}{2} + 2 \sin^2 \theta_W$
u, c, t	$\frac{1}{2}$	$\frac{2}{3}$	$\frac{1}{2}$	$\frac{1}{2} - \frac{4}{3} \sin^2 \theta_W$
d, s, b	$-\frac{1}{2}$	$-\frac{1}{3}$	$-\frac{1}{2}$	$-\frac{1}{2} + \frac{2}{3} \sin^2 \theta_W$

Table 1: Coefficients in Equation (70).

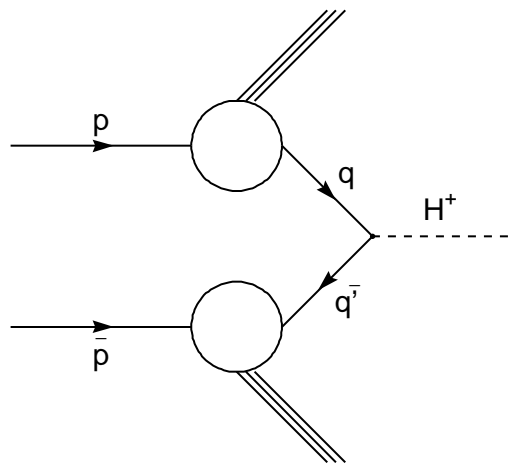


Figure 31: Feynman diagram for $p\bar{p} \rightarrow H^+X$.

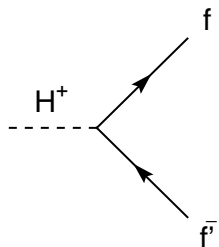


Figure 32: Feynman diagram for $H^+ \rightarrow f\bar{f}'$.

13 Production of H^+

From the diagrams in Figures 31 and 32 we obtain

$$\begin{aligned} \sigma(p\bar{p} \rightarrow H^+ X) &= \frac{4\pi^2 \gamma_H}{3m_H^3} \sum_{q,q'} \Gamma(H^+ \rightarrow q\bar{q}') \\ &\quad \int_{\gamma_A}^1 \frac{dx_a}{x_a} \left[f_q^p(x_a, m^2) \cdot f_{\bar{q}'}^{\bar{p}}\left(\frac{\gamma_H}{x_a}, m^2\right) + f_{\bar{q}'}^p(x_a, m^2) \cdot f_q^{\bar{p}}\left(\frac{\gamma_H}{x_a}, m^2\right) \right] \end{aligned} \quad (71)$$

where

$$\gamma_H = \frac{m_H^2}{s} \quad (72)$$

and

$$\begin{aligned} \Gamma(H^+ \rightarrow f\bar{f}') &= \Gamma(H^- \rightarrow f'\bar{f}) \\ &= \frac{\sqrt{2}G_F |V_{ff'}|^2 N_c}{16\pi m_H} \cdot \Lambda^{1/2} \left(\frac{m_f^2}{m_H^2}, \frac{m_{f'}^2}{m_H^2}, 1 \right) \\ &\quad \times \{ A^2 [m_H^2 - (m_f + m_{f'})^2] + B^2 [m_H^2 - (m_f - m_{f'})^2] \} \end{aligned} \quad (73)$$

with $N_c = 3$ for quarks, $N_c = 1$ for leptons,

$$A = m_{f'} \tan \beta + m_f \cot \beta \quad (74)$$

$$B = m_{f'} \tan \beta - m_f \cot \beta \quad (75)$$

$f = u, c, t, \nu_e, \nu_\mu, \nu_\tau$, and $f' = d, s, b, e^-, \mu^-, \tau^-$. [7]

14 Production of $h^0 W^+ X$

Let us now consider the channel $p\bar{p} \rightarrow h^0 W^+ X$. We obtain:

$$\begin{aligned} \frac{d^2\sigma}{dyd(p_T)^2} &= \sum_{q,q'} \int_{x_{amin}}^1 dx_a [f_q^p(x_a, m_a^2) f_{\bar{q}'}^{\bar{p}}(x_b, m_b^2) \\ &\quad + f_{\bar{q}'}^p(x_a, m_a^2) f_q^{\bar{p}}(x_b, m_b^2)] \frac{x_b \hat{s}}{m_{h^0}^2 - \hat{u}} \frac{d\sigma}{d\hat{t}} (q\bar{q}' \rightarrow h^0 W^+) \end{aligned} \quad (76)$$

where

$$f_{q'}^p = f_{q'}^p, \quad f_{\bar{q}'}^{\bar{p}} = f_q^{\bar{p}}, \quad f_{\bar{q}'}^p = f_q^p, \quad f_{q'}^{\bar{p}} = f_{\bar{q}'}^{\bar{p}}, \quad (77)$$

$$x_{amin} = \frac{\sqrt{s}m_T e^y + m_{h^0}^2 - m_W^2}{s - \sqrt{s}m_T e^{-y}}, \quad (78)$$

$$m_T = (m_W^2 + p_T^2)^{\frac{1}{2}}, \quad (79)$$

$$x_b = \frac{x_a \sqrt{s} m_T e^{-y} + m_{h^0}^2 - m_W^2}{x_a s - \sqrt{s} m_T e^y}, \quad (80)$$

$$\hat{s} = x_a x_b s, \quad (81)$$

$$p_T^2 = \frac{\Lambda(\hat{s}, m_{h^0}^2, m_W^2) \sin^2 \theta}{4\hat{s}}, \quad (82)$$

$$\hat{u} = \frac{1}{2} [m_{h^0}^2 + m_W^2 - \hat{s} - \cos \theta \Lambda^{1/2}(\hat{s}, m_{h^0}^2, m_W^2)], \quad (83)$$

$$\hat{t} = \frac{1}{2} [m_{h^0}^2 + m_W^2 - \hat{s} + \cos \theta \Lambda^{1/2}(\hat{s}, m_{h^0}^2, m_W^2)], \quad (84)$$

$$\cos \theta = \left(1 - \frac{4\hat{s}p_T^2}{\Lambda(\hat{s}, m_{h^0}^2, m_W^2)} \right)^{1/2} \quad (85)$$

and

$$\hat{u}\hat{t} = m_{h^0}^2 m_W^2 + \hat{s}p_T^2. \quad (86)$$

y is the rapidity of W^+ and p_T is the transverse momentum of W^+ . From the Feynman diagrams of Figure 6 we obtain for $f\bar{f}' \rightarrow h^0 W^+$:

$$\begin{aligned}
\frac{d\sigma}{d\hat{t}} = & \frac{1}{16\pi\hat{s}^2} |V_{ff'}|^2 G_F^2 \{ |C_{H^+}|^2 \hat{s} \Lambda \\
& \times [m_{f'}^2 \tan^2 \beta + m_f^2 \cot^2 \beta] + m_W^4 |C_W|^2 [8\hat{s}m_W^2 + \Lambda \sin^2 \theta] \\
& - 2C_{H^+} \Re(C_W) [m_{f'}^2 \tan \beta (\hat{s}\Lambda + 2m_W^2 \hat{u} (\hat{s} - m_{h^0}^2)) \\
& + 2m_W^4 (2m_{h^0}^2 - \hat{t})] - m_f^2 \cot \beta (\hat{s}\Lambda + 2m_W^2 \hat{t} (\hat{s} - m_{h^0}^2)) \\
& + 2m_W^4 (2m_{h^0}^2 - \hat{u})] \\
& + \frac{1}{2} m_W^2 \Lambda \sin^2 \theta \left[\frac{m_f^2 C_f^2}{\hat{t}^2} + \frac{m_{f'}^2 C_{f'}^2}{\hat{u}} \right] + \hat{s} [m_f^2 C_f^2 + m_{f'}^2 C_{f'}^2] \\
& + 2C_{H^+} \hat{s} \left[m_{h^0}^2 m_W^2 - \frac{1}{4} \Lambda \sin^2 \theta \right] \left[\frac{m_f^2 \cot \beta C_f}{\hat{t}} - \frac{m_{f'}^2 \tan \beta C_{f'}}{\hat{u}} \right] \\
& + 2C_{H^+} \hat{s} [m_{f'}^2 \tan \beta C_{f'} \hat{u} - m_f^2 \cot \beta C_f \hat{t}] \\
& - 2\Re(C_W) \left[\frac{1}{2} \Lambda \sin^2 \theta \left(m_W^2 + \frac{\hat{s}}{2} \right) - \hat{s} m_{h^0}^2 m_W^2 + 4\hat{s} m_W^4 + 4m_W^6 \right] \\
& \times \left[\frac{m_f^2 C_f}{\hat{t}} + \frac{m_{f'}^2 C_{f'}}{\hat{u}} \right] - 2\Re(C_W) m_f^2 C_f [-2m_W^4 + \hat{t} (\hat{s} - 2m_W^2)] \\
& - 2\Re(C_W) m_{f'}^2 C_{f'} [-2m_W^4 + \hat{u} (\hat{s} - 2m_W^2)] \} \tag{87}
\end{aligned}$$

where Λ stands for $\Lambda(\hat{s}, m_{h^0}^2, m_W^2)$,

$$C_{H^+} = \frac{\cos(\beta - \alpha)}{\hat{s} - m_H^2}, \tag{88}$$

$$C_W = \frac{\sin(\beta - \alpha) (\hat{s} - m_W^2 - im_W \Gamma_W)}{(\hat{s} - m_W^2)^2 + m_W^2 \Gamma_W^2}, \tag{89}$$

$$C_f = -\frac{\cos \alpha}{\sin \beta}, \quad C_{f'} = \frac{\sin \alpha}{\cos \beta}. \tag{90}$$

For $p\bar{p} \rightarrow h^0 W^- X$ interchange $\hat{u} \leftrightarrow \hat{t}$.

For the Standard Model we obtain the differential cross section (87) with h^0 replaced by the Standard Model higgs, $C_{H^+} = 0$, $C_f = C_{f'} = -1$, and $\sin(\beta - \alpha) = 1$ in (89).

15 Numerical examples

Two sensitive channels for the search of the Standard Model higgs are $p\bar{p} \rightarrow h^0 ZX$ and $p\bar{p} \rightarrow h^0 W^\pm X$. The cross section for $p\bar{p} \rightarrow h^0 ZX$ off resonance in

partons	$\tan(\beta) = 100$	$\tan(\beta) = 10$	$\tan(\beta) = 2$
$g\bar{g}$	0.20E+1	0.13E-1	0.35E-1
$b\bar{b}$	0.31E+2	0.31E+0	0.12E-1
$c\bar{c}$	0.73E-7	0.73E-5	0.18E-3
$s\bar{s}$	0.20E+0	0.20E-2	0.81E-4
$d\bar{d}$	0.10E-1	0.10E-3	0.41E-5
$u\bar{u}$	0.18E-9	0.18E-7	0.46E-6

Table 2: Production cross section [pb] for $p\bar{p} \rightarrow A^0$ from the indicated partons. $m_{A^0} = 200\text{GeV}/c^2$, $\sqrt{s} = 1960\text{GeV}/c^2$.

partons	$\tan(\beta) = 100$	$\tan(\beta) = 10$	$\tan(\beta) = 2$
$g\bar{g}$	0.42E+0	0.22E-2	0.19E-1
$b\bar{b}$	0.82E+1	0.82E-1	0.33E-2
$c\bar{c}$	0.19E-7	0.19E-5	0.49E-4
$s\bar{s}$	0.57E-1	0.57E-3	0.23E-4
$d\bar{d}$	0.44E-2	0.44E-4	0.18E-5
$u\bar{u}$	0.89E-10	0.89E-8	0.22E-6

Table 3: Production cross section [pb] for $p\bar{p} \rightarrow A^0$ from the indicated partons. $m_{A^0} = 250\text{GeV}/c^2$, $\sqrt{s} = 1960\text{GeV}/c^2$.

the Doublet model differs from the Standard Model by a factor $\sin^2(\beta - \alpha)$ (see Equation (70)) and it will be hard to obtain both m_{h^0} and $\tan(\beta)$. We are therefore interested in the production of h^0Z on resonance. In particular $p\bar{p} \rightarrow A^0$ followed by $A^0 \rightarrow h^0Z \rightarrow b\bar{b}l^-l^+$ where $l = \mu, e$. A peak should be observed in the h^0Z invariant mass. From Equation (61) we obtain the cross sections listed in Tables 2 and 3.

Let us now consider the decays of A^0 . As an example we take $m_{h^0} = 120\text{GeV}/c^2$, $m_{H^0} = 250\text{GeV}/c^2$, $m_H = 200\text{GeV}/c^2$ and $m_{A^0} = 250\text{GeV}/c^2$. The corresponding branching fractions are listed in Table 4. From Tables 3 and 4 we obtain a production cross section times branching fraction for the process $p\bar{p} \rightarrow A^0 \rightarrow h^0Z$ of 0.018pb for $\tan(\beta) = 2$, and 0.0045pb for $\tan(\beta) = 10$.

From Equations (71) and (73) we obtain the production cross sections for $p\bar{p} \rightarrow H^+X$ shown in Table 5.

Other channels of experimental interest are the production of 3 or more b -jets as in Figure 33. Some numerical calculations using the CompHEP program[8] are presented in Table 6.

partons	$\tan(\beta) = 100$	$\tan(\beta) = 10$	$\tan(\beta) = 2$
$A \rightarrow gg$	3.0E-4	1.5E-4	2.0E-3
$A \rightarrow b\bar{b}$	1.0E+0	9.4E-1	5.9E-2
$A \rightarrow c\bar{c}$	8.0E-10	7.5E-6	2.9E-4
$A \rightarrow s\bar{s}$	8.0E-4	7.5E-4	4.7E-5
$A \rightarrow Zh^0$	6.1E-6	5.5E-2	9.4E-1
$A \rightarrow Z\gamma$	1.9E-8	6.0E-9	1.2E-6
$A \rightarrow \gamma\gamma$	1.2E-7	8.1E-8	7.5E-6

Table 4: Branching fractions for A^0 assuming $m_H = 200\text{GeV}/c^2$, $m_{H^0} = 250\text{GeV}/c^2$, $m_{A^0} = 250\text{GeV}/c^2$ and $m_{h^0} = 120\text{GeV}/c^2$.

partons	$\tan(\beta) = 100$	$\tan(\beta) = 10$	$\tan(\beta) = 2$
ud	0.82E-2	0.82E-4	0.34E-5
$u\bar{s}$	0.66E-1	0.66E-3	0.26E-4
$u\bar{b}$	0.89E-2	0.89E-4	0.36E-5
$c\bar{s}$	0.31E-1	0.32E-3	0.91E-4
$c\bar{b}$	0.24E-1	0.24E-3	0.96E-5

Table 5: Production cross section [pb] for $p\bar{p} \rightarrow H^+X$ from the indicated partons. $m_{H^0} = 250\text{GeV}/c^2$, $\sqrt{s} = 1960\text{GeV}/c^2$.

process	$\tan(\beta) = 100$	$\tan(\beta) = 50$	$\tan(\beta) = 2$
$b + g \rightarrow b + h^0$	0.021	0.021	0.011
$u + \bar{u} \rightarrow b + \bar{b} + h^0$	0.002	0.001	0.0004
$d + \bar{d} \rightarrow b + \bar{b} + h^0$	0.0005	0.0005	0.0001
$g + g \rightarrow b + \bar{b} + h^0$	0.015	0.015	0.008

Table 6: Production cross section [pb] for $p\bar{p} \rightarrow bh^0X$ from the indicated processes. $m_{h^0} = 120\text{GeV}/c^2$, $m_{A^0} = 250\text{GeV}/c^2$, $\sqrt{s} = 1960\text{GeV}/c^2$.

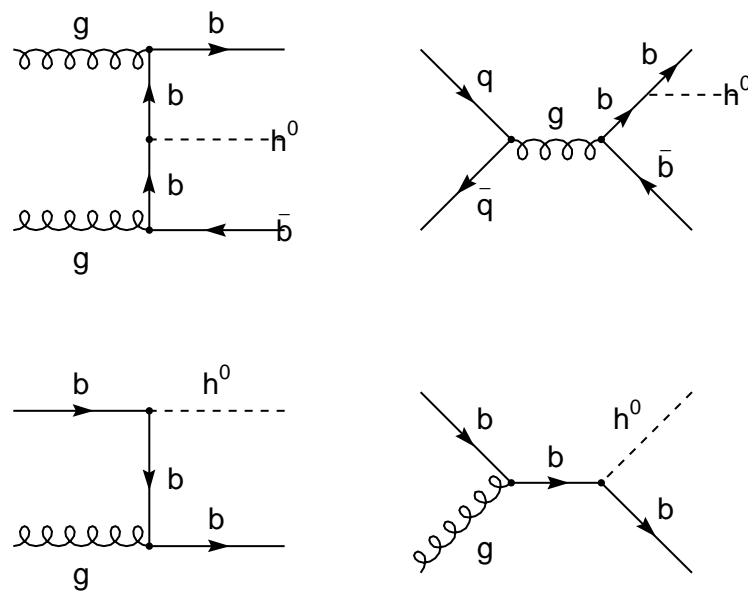


Figure 33: Some Feynman diagrams for the production of three or more b -jets.

16 Running coupling constants and Grand Unification

The coupling constants of the Two Higgs Doublet Model of type II are $g_s(\mu)$ for $SU(3)$, $g(\mu)$ for $SU(2)$, and $g'(\mu)$ for $U(1)$. These coupling constants depend on the energy scale μ as follows:

$$\frac{1}{g_s^2(\mu)} = \frac{1}{g_s^2(m_x)} + \frac{1}{8\pi^2} \left(-11 + \frac{4}{3}n_F \right) \ln \left(\frac{m_x}{\mu} \right), \quad (91)$$

$$\frac{1}{g^2(\mu)} = \frac{1}{g^2(m_x)} + \frac{1}{8\pi^2} \left(-\frac{22}{3} + \frac{4}{3}n_F + \frac{1}{6}n_S \right) \ln \left(\frac{m_x}{\mu} \right), \quad (92)$$

$$\frac{1}{g'^2(\mu)} = \frac{1}{g'^2(m_x)} + \frac{1}{8\pi^2} \left(\frac{20}{9}n_F + \frac{1}{6}n_S \right) \ln \left(\frac{m_x}{\mu} \right), \quad (93)$$

where n_F is the number of families of quarks and leptons, and n_S is the number of higgs doublets. For the Two Higgs Doublet Model of type II considered in this article, $n_F = 3$ and $n_S = 2$. In terms of the elementary electric charge and the Weinberg angle, $g(m_Z) = e(m_Z)/\sin\theta_W(m_Z)$, $g'(m_Z) = e(m_Z)/\cos\theta_W(m_Z)$. The fine structure constant is $\alpha(m_Z) = e^2(m_Z)/(4\pi)$.

Let us now assume that a Grand Unified Theory (GUT) breaks its symmetry to $SU(3) \times SU(2) \times U(1)$ at the energy scale m_x . At this scale we take

$$g_s^2(m_x) = g^2(m_x) = \frac{5}{3}g'^2(m_x), \quad (94)$$

and obtain

$$\sin^2\theta_W = \frac{11 + \frac{1}{2}n_S + \frac{5e^2}{3g_s^2} (22 - \frac{1}{5}n_S)}{66 + n_S}, \quad (95)$$

$$\ln \left(\frac{m_x}{m_Z} \right) = \frac{24\pi^2}{e^2} \frac{1 - \frac{8e^2}{3g_s^2}}{66 + n_S}, \quad (96)$$

with all running couplings evaluated at m_Z .

The corresponding equations of the Minimum Supersymmetry Model[9] are

$$\sin^2\theta_W = \frac{18 + 3n_S + \frac{e^2}{g_s^2} (60 - 2n_S)}{108 + 6n_S}, \quad (97)$$

$$\ln \left(\frac{m_x}{m_Z} \right) = \frac{8\pi^2}{e^2} \left[\frac{1 - \frac{8e^2}{3g_s^2}}{18 + n_S} \right]. \quad (98)$$

n_S	Doublet Model		MSSM	
	$\sin^2 \theta_W(m_Z)$	m_x	$\sin^2 \theta_W(m_Z)$	m_x
0	0.2037	$1.0 \cdot 10^{15}$	0.2037	$8.0 \cdot 10^{17}$
2	0.2118	$4.2 \cdot 10^{14}$	0.2311	$2.0 \cdot 10^{16}$
4	0.2194	$1.8 \cdot 10^{14}$	0.2536	$1.0 \cdot 10^{15}$
6	0.2266	$8.3 \cdot 10^{13}$	0.2722	$8.3 \cdot 10^{13}$
8	0.2334	$3.9 \cdot 10^{13}$	0.2880	$1.0 \cdot 10^{13}$

Table 7: Predicted $\sin^2 \theta_W(m_Z)$ and m_x for the Two Higgs Doublet Model of type II, and the Minimum Supersymmetric Model as a function of the number of doublets n_S .

Some numerical results are presented in Table 7. From the Table we conclude that the Two Higgs Doublet Model of type II is in disagreement with the measured value of $\sin^2 \theta_W(m_Z)$, and with the non-observation of proton decay (m_x is too low). Raising the number of doublets to ≈ 7 would bring $\sin^2 \theta_W(m_Z)$ into agreement with observations, but m_x is still too low. The MSSM with $n_S = 2$ (which includes the Two Higgs Doublet Model of type II) is in agreement with both the observed $\sin^2 \theta_W(m_Z)$, and with the non-observation of proton decay.

17 Conclusions

One of the major efforts at the Fermilab Tevatron in Run II, and at the future LHC, is the search for the Standard Model higgs h_{SM} . The four channels with largest production cross section are[6] $gg \rightarrow h_{SM}$, $q\bar{q}' \rightarrow h_{SM}W$, $q\bar{q} \rightarrow h_{SM}Z$ and $q\bar{q} \rightarrow h_{SM}q\bar{q}$. The decay modes of h_{SM} with largest branching fraction[6] are $b\bar{b}$ for $m_h \lesssim 137\text{GeV}$ and W^+W^- for $m_h \gtrsim 137\text{GeV}$.

The search for the Standard Model higgs will also constrain or discover particles of the Two Higgs Doublet Model of type II.

The most interesting production channels are $gg \rightarrow h^0, H^0, A^0$ on mass shell, and $q\bar{q}, gg \rightarrow h^0Z$ and $q\bar{q}' \rightarrow h^0W^\pm$ in the continuum (tho there may be peaks at m_{A^0}). The most interesting decays are $h^0, H^0, A^0 \rightarrow b\bar{b}$ -jets and $\tau^+\tau^-$, and, if above threshold, $H^0 \rightarrow ZZ$, W^+W^- and h^0h^0 . The following final states should be compared with the Standard Model cross section: $b\bar{b}Z$, $b\bar{b}W^\pm$, $\tau^+\tau^-Z$, $\tau^+\tau^-W^\pm$, $b\bar{b}$, $\tau^+\tau^-$, ZZ , W^+W^- , 3 and 4 b -jets, $2\tau^+ + 2\tau^-$, $b\bar{b}\tau^+\tau^-$, ZW^+W^- , $3Z$, ZZW^\pm and $3W^\pm$. Mass peaks should be searched in the following channels: $Zb\bar{b}$, ZZ , ZZZ , $b\bar{b}$, 4 b -jets and, just in case, $Z\gamma$.

We have discussed the masses of the higgs particles in the Two Higgs

Doublet Model of type II, and have calculated several relevant production and decay rates. We have also discussed running coupling constants and Grand Unification. If the Two Higgs Doublet Model of type II is part of a Grand Unified Theory, then it does not agree with the observed $\sin^2 \theta_W$ nor with the non-observation of proton decay. The MSSM with $n_S = 2$ (which includes the Two Higgs Doublet Model of type II) is in agreement with both the observed $\sin^2 \theta_W(m_Z)$, and with the non-observation of proton decay.

References

- [1] Vernon Barger and Roger Phillips, *Collider Physics* (Addison Wesley, 1988), pages 452-454; S. Dawson, J. F. Gunion, H.E. Haber and G. Kane, *The Higgs Hunter's Guide* (Addison Wesley, 1990), p. 201.
- [2] Carlos A. Marín and Bruce Hoeneisen, hep-ph/0210167 (2002).
- [3] CDF Collab., Phys. Rev. Lett. **79**, 357 (1997).
- [4] D0 Collab., Phys. Rev. Lett. **82**, 4975 (1999); FERMILAB-Conf-00-294-E.
- [5] LEP Higgs Working Group, <http://lephiggs.web.cern.ch/LEPHIGGS/papers/index.html>; LHWG Note/2001-05.
- [6] *Review of Particle Physics*, K. Hagiwara *et al*, Physical Review **D66**, 010001 (2002).
- [7] Carlos Marín y Guillermo Hernández, Serie de Documentos USFQ **13**, Universidad San Francisco de Quito, Ecuador (1994)
- [8] “CompHEP: A package for evaluation of Feynman diagrams and integration over multiparticle phase space.” A. Pukhov, E. Boos, M. Dubinin, V. Edneral, V. Ilyin, D. Kovalenko, A. Kryukov, V. Savrin, S. Shichanin, A. Semenov, hep-ph/9908288 (1999)
- [9] “The quantum theory of fields”, Volume III, Supersymmetry, Steven Weinberg, Cambridge University Press (2000).